HHS Public Access

Author manuscript

J Labelled Comp Radiopharm. Author manuscript; available in PMC 2019 July 01.

Published in final edited form as:

J Labelled Comp Radiopharm. 2018 July ; 61(9): 727–738. doi:10.1002/jlcr.3605.

^{89}Zr-ImmunoPET Companion Diagnostics and their Impact in Clinical Drug Development

Brooke N. McKnight[1] and **Nerissa T. Viola-Villegas**[2]

[1]Cancer Biology, Wayne State University School of Medicine, Detroit, MI 48201

[2]Department of Oncology, Karmanos Cancer Institute, Detroit, MI 48201

Abstract

Therapeutic monoclonal antibodies (mAbs) have been used in cancer treatment for 30 years, with around 24 mAb and mAb:drug conjugates approved by the FDA to date. Despite their specificity, efficacy has remained limited, which, in part, derails nascent initiatives towards precision medicine. An image-guided approach to reinforce treatment decisions using immune positron emission tomography (immunoPET) companion diagnostic is warranted. This review provides a general overview of current translational research using Zr-89 immunoPET and opportunities for utilizing and harnessing this tool to its full potential. Patient case studies are cited to illustrate immunoPET probes as tools for profiling molecular signatures. Discussions on its utility in reinforcing clinical decisions as it relates to histopathological tumor assessment and standard diagnostic methods, and its potential as predictive biomarkers are presented. We finally conclude with an overview of practical considerations to its utility in the clinic.

Keywords

ImmunoPET; companion diagnostics; antibody; imaging; clinical trials

Introduction

Therapeutic monoclonal antibodies (mAbs) gained clinical utility in 1985 with the first US Food and Drug Administration (FDA)-approval of the biologic, muromonab-CD3 (Orthoclone™ OKT3), specific for cluster of differentiation (CD3), a co-receptor present on all T-cells[1]. Since then, applications in cancer have been exploited with the approval of rituximab (anti-CD20) in 1997[2] followed by trastuzumab (anti-HER2) in 1998[3]. By 2016, there were 24 mAbs and antibody drug conjugates (ADC) approved by the FDA for cancer treatment. These mAbs are directed to a specific target ranging from tumor and cell-surface associated antigens to biomarker signatures within the tumor microenvironment. Despite their specificity and moderate safety profile, clinical efficacy of these mAbs remains limited due to perpetuating factors, including but not limited to i) unpredictable tumor antigen density, ii) internalizing status of the mAb:antigen complex, iii) target hit rate, iv) vascular

*Corresponding Author: Nerissa T. Viola-Villegas, Ph.D., Department of Oncology, Karmanos Cancer Institute, 4100 John R street, Detroit, MI, 48201, Tel: (313)576-8309, Fax: (313)576-8928, villegan@karmanos.org.

Disclosure: The authors do not have conflicts of interest.

penetration, and, v) tissue distribution, which may impact adverse events[4–8]. All of these factors underscore the need for precision medicine, borne out of the intent of tailoring the disease treatment and prevention by providing the right drug to the right patient at the appropriate time and dose. A logical approach to precision medicine explores non-invasive imaging tools that can be repeatedly utilized to profile tumors at the molecular level, and to augment flaws present in biopsies. With this perspective, antibody or immune-based positron emission tomography (immunoPET) was developed to provide a direct readout of antigen density present within each lesion; moreover, the pharmacokinetic and dosimetric properties of the mAb, in the case of radioimmunotherapy, can be considered cognate when compared to the imaging tool[9]. Taken together, immunoPET has a high potential to influence and direct informed decisions in drug design and development. In this review, we present a general overview of immunoPET, specifically imaging agents labeled with ^{89}Zr while briefly touching on tracer development. We discuss the clinical impact of ^{89}Zr-immunoPET, its role in drug development and factors to consider to harness its utility as an effective companion diagnostic (CDx).

ImmunoPET tracer development

The development of immunoPET tracers relies on the following principles: i) the biological and chemical properties of the mAb, ii) the radionuclide chosen iii) the chelate selected, and iv) the stability of the linker between mAb and chelate. MAbs for patient use are either humanized or made fully human to prevent human anti-mouse antibody response (HAMA)[10]. The size of full-length biologics (~150 kDa) prolongs their half-life in the blood, which affects the length of delivery to the tumor target and clearance from healthy tissues. Thus, pairing with long-lived radionuclides ^{64}Cu ($t_{1/2}$ ~ 12.7 h), ^{86}Y ($t_{1/2}$ ~ 14.7 h), ^{89}Zr ($t_{1/2}$ ~ 78.4 h), and ^{124}I ($t_{1/2}$ ~ 100.3 h) is the most common strategy[11]. Matching the physical and biological half-lives of the PET nuclide and the mAb, respectively, ensures that the probe accumulates in the tumor before the radioactivity decays and further allows clearance from normal tissues. In this regard, enhanced signal-to-noise ratio – one of the primary considerations in diagnostic imaging – is achieved.

One limitation to using full mAbs specifically for imaging purposes is the long wait times between tracer administration and imaging acquisition, as well as non-trivial dose exposure of non-target organs. Tracer pharmacokinetics can be improved by decreasing its size, effectively reducing circulation time, and minimizing dose exposure to the patient[12]. With this perspective, smaller fragment constructs are engineered offering shorter blood residencies and faster tumor target delivery[10]. These fragments mostly retain the variable region where the antigen-binding site is primarily located. Suggested PET radionuclide tags to complement mAb fragments are provided in Table 1. Moderately-sized fragments (i.e. F(ab)'2 (~100–110 kDa), minibody (~75 kDa), and diabody (~50 kDa)) may be appropriately labeled with ^{18}F ($t_{1/2}$ ~ 109 min), ^{64}Cu ($t_{1/2}$ ~ 12.7 h) and ^{86}Y ($t_{1/2}$ ~ 14.7 h). Smaller-sized fragments like affibodies (~ 6 kDa), nanobodies or single domain antibodies (~12–15 kDa) can be radiolabeled with shorter-lived isotopes like ^{18}F and ^{68}Ga ($t_{1/2}$ ~ 68 min), which consequently decreases the radiation exposure of the patient[13]. The caveat herein lies in the overall rate of clearance and nuclide site delivery of the mAb fragments.

Zirconium-89 immunoPET tracers

Standardized production and commercial availability has made the development of Zr-89 radiolabeled mAbs relatively straightforward[14–15]. As a radiometal, Zr-89 requires complexation to prevent random, non-specific binding to non-targeted tissue (usually the bone), which consequently lowers contrast[16]. To date, only desferrioxamine (DFO), a known iron-sequestering siderophore with three hydroxamate groups is currently utilized as a chelate despite reports of metal:complex *in vivo* instability[17–18]. DFO bioconjugation techniques were established either through non-specific attachment to terminal lysines[19–20] and cysteines[13] or through a more discriminate glycan selective labeling[21]. Consequently, preclinical research flourished with many imaging probes developed to target different oncogenic molecular signatures. A significant number of these tracers were developed to target surface-bound biomarkers, such as i) members of the epidermal growth factor receptor family (e.g. EGFR[22], HER2[23] and HER3[24]), ii) prostate-specific membrane antigen (PSMA)[25], iii) prostate stem cell antigen (PSCA)[26], iv) CD20[27], v) CD44[28], vi) programmed death receptor (PD1)[29] and vii) programmed death ligand 1 (PD-L1)[30], to name a few. Imaging probes targeting secreted signaling proteins (e.g. VEGF, granzyme B, interferon-γ)[31–33], antigen/receptors bound to T cells (e.g. CD3[34], CD8[35]) and shed antigens (e.g. CA19.9[36], carcinoembryonic antigen or CEA[37]) were also investigated. With substantial preclinical data, a number of these tracers have progressed to clinical trials. The first study of a ^{89}Zr-mAb probe (^{89}Zr-cmAb U36) targeting CD44v6 in patients with head and neck cancer was reported in 2006[38]. The number of ^{89}Zr-based immunoPET probes in the clinic tripled in 2013[17] As of this writing, to the best of our knowledge and after extensive search at clinicaltrials.gov, there are ~22 ^{89}Zr-mAbs that are currently undergoing or have completed patient trials. An overview of ^{89}Zr-based immunoPET probes can be found in Table 2.

The Clinical Impact of ImmunoPET Companion Diagnostics

Molecular profiling of lesions

Understanding the molecular profile of the malignancy is necessary to determine treatment indications. A standard clinical strategy obtains tumor specimens through surgical or core needle biopsies in solid tumors for histopathological analyses. Liquid biopsies are also obtained from blood, urine, sputum, or cerebrospinal fluid, which carry shed or circulating biomarkers[39]. Biopsy-driven molecular profiling is often fraught with problems and disadvantages since access to the tumor sites may be difficult, often requiring complicated invasive procedures[40]. Tumor heterogeneity renders biopsies inconsistent, which can inadequately portray the presence and level of expression of the molecular signature; thus, requiring more tests to accurately characterize the tumor. Consequently, proper histopathological analysis of the receptor/antigen density may not be reflected, potentially eliminating a patient from benefiting from molecular-based treatments. Repeat biopsies are performed on patients to pathologically confirm malignancy to direct treatment decisions, but secondary biopsy results may not match the original pathology report[41]. Moreover, multiple sequential biopsies are deemed impractical, unethical, and unsafe[41]. In this regard, using a PET probe to profile tumors could reduce cases of biopsy mismatch by looking at the entire tumor in an unperturbed, non-invasive setting. In the succeeding sections, the

benefits and considerations are discussed using patient case studies reported in recent years as examples.

Confirmation of malignancy and antigen density

ImmunoPET may potentially provide an image-guided molecular diagnostic tool where pathological results may not be able to confirm and identify true positive disease. It detects the target antigen and quantitatively measures its expression. The imaging agent ^{18}F-FDG has long been the standard PET tracer for detecting lesions, but it is limited to visualizing tumor metabolism. Moreover, weak tumor avidity or probe accumulation, non-specific tissue binding, and low metabolic lesions can pose problems, hindering detection[42]. Pandit-Taskar *et al.* conducted identification of metastatic bony lesions using the anti-PSMA PET tracer, ^{89}Zr-J591 and analyzed against lesions detected by ^{18}F-FDG, bone scans (^{99m}Tc-medronic acid (MDP)) and computed tomography (CT). ^{89}Zr-J591 was able to detect four occult lesions, which were undetected by FDG and other imaging assays[43]. Out of 21 lesions, 19 were PSMA-positive as identified by ^{89}Zr-J591. Of these select osseous lesions, two were biopsy-proven negative, but further assessment using magnetic resonance imaging confirmed one of the lesions as metastatic with a repeat biopsy confirming the malignancy.

Optimization of pharmacokinetics

Admittedly, utility of full-length mAb as vectors of PET nuclides are limited. The long-lived blood pool circulation of these mAbs (3–8 days) yield long wait times between administration and scan acquisitions for optimum contrast between tumor and normal tissue signal. In this regard, antibody fragments are currently explored as faster alternatives. A prospective phase I/IIa clinical trial investigating ^{89}Zr-IAB2M, a minibody targeting PSMA in metastatic prostate cancer proved this principle (Fig. 1A-C)[44]. A comparison of the pharmacokinetic properties between ^{89}Zr-J591 and the minibody tracer displayed faster serum clearance of the latter (Fig. 1D) with lesion accumulation at 24–48 hours (^{89}Zr-J591: 6–8 days after administration, Fig. 1E). Organ dosimetries were parallel for both tracers with hepatic tissue attaining the highest dose exposure.

Receptor occupancy and pharmacokinetics dose validation

Dose escalation studies using ^{89}Zr-IAB2M (anti-PSMA minibody) in patients were conducted with 10 mg, 20 mg, or 50 mg of IAB2M. Differences in biodistribution were minor across all doses. Decreased blood pool activity coupled with an increased liver and GI tract accumulation was observed over time. The highest lesion uptake was seen in the 10-mg cohort with optimal biodistribution for imaging, as well as improved delineation of bony metastatic sites. Of note, increased doses of the cold IAB2M resulted in slower serum clearance due to mass effects, although a non-significant decrease in liver uptake was noted in the 50 mg cohort. Perhaps the most impact immunoPET has contributed can be gleaned from the pioneering study investigating the biodistribution of ^{89}Zr-trastuzumab in patients with metastatic breast cancer (BC). Djikers *et al.* observed rapid hepatic excretion and low blood pool levels of the tracer in breast cancer (BC) patients who are naïve to trastuzumab with extensive HER2+ tumor mass in the liver; consequently, a false-negative readouts in distal metastatic sites was exhibited[45]. The hepatic “sink” and poor uptake in metastatic lesions were attributed to slow extravasation of the drug through the vascular compartment

compared to fast pharmacokinetic clearance of the mAb at low dose levels. In this study, a 10 and 50 mg loaded dose displayed terminal half-lives of 1.5 and 4.3 days respectively; in contrast, tumor penetration and accumulation of ^{89}Zr-trastuzumab occurred between 4–5 days. To gain perspective, administered therapeutic doses (4 mg/kg loading plus 2 mg/kg maintenance dose) reached an average terminal half-life of ~28.5 days when at steady state. Another important finding of this pivotal clinical trial was the importance of drug receptor occupancy. The fast pharmacokinetics of low trastuzumab doses led the authors to estimate drug/receptor occupancy by considering the amount of HER2 per tumor cell and the liver mass of the patient. The mass (1.2 kg) was obtained through image analysis of normalized PET/CT scans. The authors rationalized that a 50 mg dose of trastuzumab, equivalent to 2.0×10^{17} trastuzumab molecules (via conversion through Avogadro's number) cannot fully saturate over a kg (1.2 kg) of tumor tissue based on the following approximations. A gram of tumor tissue is nearly comprised of ~1×10^9 cells. Each single cell, on average, possesses 2 million HER2 receptor sites. Thus, in the patient's case, there are ~2.4×10^{18} HER2 receptor molecules present in the hepatic metastases, 10-fold higher than the 50 mg dose (1.2×10^3 g tumor tissue × 1×10^9 cells/g × 2×10^6 HER2 receptors/cell)[46–47]. Majority of the dose (50 mg) accumulated in the extensive liver metastasis. This created the impetus to vary doses in patients who are naïve to trastuzumab versus those receiving this treatment with the former requiring more mAb administered (50 mg vs. 10 mg, respectively, Fig. 2).

Taken together, these pivotal biodistribution studies underscore the substantial dependence of mAb-based therapies (e.g. trastuzumab-emtansine (T-DM1)[48], pertuzumab[49], rituximab[50]) on pharmacokinetics for personalized dosing strategies. Current clinical protocol relies on body weight to determine drug doses administered. ImmunoPET CDx can potentially transform this practice by facilitating the assessment of effective patient-tailored doses based on the extent of tumor burden and mAb pharmacokinetics.

Discordance with pathologic findings

A clinical study assessing ^{89}Zr-rituximab as an imaging biomarker of CD20 in patients with relapsed or refractory diffuse large B cell lymphoma was correlated against pathologic findings[51]. Biopsy-proven lesions (5/6 patients) showed concordance with the tumor uptake of ^{89}Zr-rituximab. A strong uniform staining of CD20 was correlated with a high SUV_{peak} of 12.8 while a moderate, heterogeneous CD20 expression corresponded to a tumor uptake of SUV_{peak} ~ 3.2–5.4 (Fig. 3A). In certain cases, the pathology may lead to discordance with the immunoPET data. One patient demonstrated a biopsy-mismatch with CD20 PET displaying a positive tumor uptake (SUV_{peak} ~ 3.8) but negative pathology (Fig. 3B). The lesion was conclusively assessed as a true positive.

Another concrete example was presented by Ulaner *et al.* investigating HER2-PET in patients with HER2-negative primary BC[52]. Of the 20 patients, 15% (3/20) were identified by ^{89}Zr-trastuzumab as having unsuspected HER2-positive metastases with proven pathologies. In Fig. 4, a patient who was diagnosed with ER+/HER2- invasive ductal BC presented two years later with several bone lesions and was observed HER2-PET avid. Biopsy of the right ilium (SUV~ 5.9) confirmed metastases but with an ambiguous IHC score of 2+. Confirmation of the foci as true-positive was made using MSK-IMPACT assay.

Of note, the authors emphasized that the intensity of the PET tracer on foci can indiscriminately assess true- from false-positive lesions. The study reported ~30% (6/20) of the patient population was conservatively categorized as false-negative due to negative pathology even with foci avidity for the probe. The relatively high incidence of false-positive lesions was attributed to non-specific uptake of free Zr-89, particularly in osseous sites, which marginalizes the use of this nuclide for detecting bone metastases. Collectively, tumor heterogeneity can impact go/no-go treatment decisions with standard biopsy results rendering ambiguity to some extent. In these cases, immunoPET can reinforce and potentially resolve equivocal tumor pathology. However, confirmation of true-positive or -negative lesions as visualized by immunoPET needs to be meticulously validated.

Tissue distribution, radiation dosimetry and the need for sequential imaging

PET-derivatized mAbs can be utilized to determine distribution and organ exposure. This strategy has been utilized several years ago especially in the field of radioimmunotherapy. Isotopologues like ^{111}In/^{177}Lu[53], ^{111}In/^{90}Y)[54] and ^{99m}Tc/^{186}Re[55] are ideal radionuclides as theranostics (imaging and drug agents developed in tandem)[56]. Unfortunately, zirconium-89, the ideal PET nuclide for mAb radiochemistry does not have a therapeutic isotopologue nuclide[13,57] albeit zirconium has two other beta-emitting radioisotopes, ^{95}Zr ($t_{1/2}$ ~ 64.0 d) and ^{97}Zr ($t_{1/2}$ ~ 16.74 h) that could potentially be useful but have not been investigated. Despite this limitation, a number of studies continued to employ ^{89}Zr for tissue distribution and dosimetry studies owing to its inherent properties as a PET nuclide. This was evident in a study, which demonstrated ^{89}Zr-ibritumomab tiuxetan as a far better tool for evaluating distribution and dosimetry of ^{90}Y-labeled ibritumomab tiuxetan (Zevalin™), compared to using the single photon emission tomography (SPECT) isotope-labeled counterparts (e.g. ^{111}In and ^{131}I)[58]. Using SPECT can be problematic and prone to errors stemming from its lower sensitivity with low geometric efficiencies (~0.01% detected vs. emitted photons) as a consequence of its poor collimator detector response[59]; thus, requiring substantial correction and compensation algorithms to achieve accurate quantification for dose-toxicity assessments[60]. The study was conducted in patients with non-Hodgkins lymphoma who were given the tracer either for baseline imaging or during Zevalin treatment. Tissue binding and clearance were observed in a manner consistent with the radioimmunotherapy with a slight difference in bone uptake. Disparities in organ and whole body absorbed dose estimations are apparent when compared to SPECT-labeled ibritumomab tiuxetan. In the ^{89}Zr-labeled mAb, the organ receiving the highest dose was the liver (3.2 ± 1.8 mGy/MBq) followed by the spleen (2.9 ± 0.7 mGy/MBq) with a whole body absorbed dose of 0.87 mSv/MBq. Several studies utilizing ^{111}In-labeled ibritumomab tiuxetan showed a reversed trend, with the spleen absorbing the highest dose followed by the liver. A study by Carrasquillo *et al.* revealed that pharmacokinetic parameters between ^{111}In and ^{90}Y differ by ~10–15%, which can account for dosimetry differences[61].

The findings from this study outline the advantages of ^{89}Zr-immunoPET over SPECT-based CDx to recapitulate whole body distribution of its radioimmunotherapy counterpart. Utilizing CDx further extracts dose-response correlations to determine drug efficacy and toxicities.

Predictive markers of treatment

A first-in-human study investigated by Lamberts et al. evaluated ^{89}Zr-MMOT0530A in pancreatic tumors and metastases expressing mesothelin (MSLN)[62]. Pre-treatment scans showed a mean SUV_{max} of 11.5 ± 5.6 lesions in the pancreas. Patients received the antibody-drug conjugate DMOT4039A (MMOT0530A bound to MMAE) followed by ^{89}Zr-MMOT0530A PET, 4 days post injection of the tracer. After treatment, 9 out of 11 patients presented with stable disease, and two patients had progressive disease. Those with progressive disease showed an uptake in liver metastasis with the PET tracer. This suggests that ^{89}Zr-MMOT0530A-PET can be used to visualize pancreatic cancer lesions, as well as guide individualized antibody-based treatment with the ADC DMOT4039A.

The landmark ZEPHIR study evaluated the predictive value of HER2 PET/CT in combination with FDG PET prior to T-DM1 treatment in patients with metastatic breast cancer[63]. From the 55 patients enrolled, 16 (29%) were negative for HER2-PET while 39 patients were categorically classified as positive for HER2-PET/CT, depending on lesion heterogeneity. From the HER2-positive pool, 28 patients displayed an objective response (OR) after 3 cycles of T-DM1. In combination with post-treatment (after 1 cycle of T-DM1), a 100% positive predictive value (PPV) was achieved for HER2-PET imaging (72% PPV) in combination with early treatment FDG-PET imaging based on RECIST 1.1 (Fig. 5). Moreover, a time-to-treatment failure of ~ 11.2 months in the HER2-positive group and ~3.5 months for the HER2-negative group were identified. A negative predictive value of 88% in patients with low HER2-PET was deemed clinically significant. To date, this is the first trial that used a three-prong strategy that employed imaging biomarkers for go/no go treatment decisions in the clinic. In conclusion, these clinical trials highlighted the potential of immunoPET to measure functional effects of targeted treatment, making this imaging technique a conceivable predictive and prognostic biomarker.

Practical Considerations

While immunoPET CDx may seem straightforward, several aspects of using this imaging technique need to be deliberated. The amount of dose administered and the interval between tracer administration and imaging acquisition warrant investigation to obtain an optimized contrast between lesions and background. In the case of ^{89}Zr-trastuzumab, the optimal imaging time for a ~37 MBq (50 mg) intravenous injection was observed between 4–5 days after injection[45,65]. At this period, low blood pool activity and high tumor avidity was established. Imaging at longer periods >6 days can compromise the spatial resolution and image quality[45]. At higher activities (~185 MBq/50 mg) administered, ^{89}Zr-trastuzumab still generated high quality spatial resolution in images acquired between 5–6 days post-injection[45,51–52,64–65]. The scan periods of 4–6 days depending on the dose are typical for other full-length mAb tracers in clinical trials. For smaller biologics-based tracers, ^{89}Zr-IAB2M, for example, demonstrated shorter interval wait times with the best lesion to background ratio identified at 48 h p.i.[44] Safety profiles of ^{89}Zr-labeled mAbs require careful assessment to limit radiation-related toxicities. Whole body effective doses reported in a number of early phase studies ranged from 0.41 mSv/MBq for ^{89}Zr-IAB2M[45], 0.87 ± 0.14 mSv/MBq for ^{89}Zr-ibritumomab tiuxetan[58], 0.47 mSv/MBq for ^{89}Zr-trastuzumab[66]

and 0.264 mSv/MBq for ^{89}Zr-panitumumab[67] whereas FDG-PET[68] had a reported mean effective dose of 0.0199 ± 0.0032 mSv/MBq.

Engagement of immunoPET CDx as predictive imaging biomarkers in the clinic should continuously be explored to support clinical translational efforts towards precision medicine. It has already shown beneficial in accurately profiling lesions at the molecular level when pathology is incorrect, discovering the density of targets available, and determining the biodistribution of therapy before treating the patient. Sequential imaging in test-retest studies can provide a viable tool to appropriately dose patients, but should be used with caution during treatment regimens. In a nutshell, immunoPET is still at its early stages of clinical development and will most likely require further standardization (i.e. streamlined SUV readout analysis, chemistry optimization) and validation through other molecular profiling tools. Once harnessed, its benefits can provide a powerful impact in patient management.

Acknowledgments

The authors would like to acknowledge NIH R00 CA181492 (NTVV) and T32 CAA09531 (BNM) for financial support.

References

1. Van Wauwe JP, De Mey JR, Goossens JG. OKT3: a monoclonal anti-human T lymphocyte antibody with potent mitogenic properties. J Immunol. 1980; 124(6):2708–2713. [PubMed: 6966296]
2. Grillo-Lopez AJ, White CA, Dallaire BK, Varns CL, Shen CD, Wei A, et al. Rituximab: the first monoclonal antibody approved for the treatment of lymphoma. Curr Pharm Biotechnol. 2000; 1(1): 1–9. [PubMed: 11467356]
3. Slamon DJ, Leyland-Jones B, Shak S, Funchs H, Paton V, Bajamonde A, Fleming T, Eiermann W, Wolter J, Pegram M, Baselga J, Norton L. Use of Chemotherapy plus a Monoclonal Antibody against HER2 for Metastatic Breast Cancer That Overexpresses HER2. NEJM. 2001; 344:783–792. [PubMed: 11248153]
4. Perez HL, Cardarelli PM, Deshpande S, Gangwar S, Schroeder GM, Vite GD, et al. Antibody-drug conjugates: current status and future directions. Drug Discov Today. 2014; 19(7):869–81. [PubMed: 24239727]
5. Shah DK, Haddish-Berhane N, Betts A. Bench to bedside translation of antibody drug conjugates using a multiscale mechanistic PK/PD model: a case study with brentuximab-vedotin. J Pharmacokinet Pharmacodyn. 2012; 39(6):643–59. [PubMed: 23151991]
6. Vasalou C, Helmlinger G, Gomes B. A mechanistic tumor penetration model to guide antibody drug conjugate design. PloS one. 2015; 10(3):e0118977. [PubMed: 25786126]
7. Kovtun YV, Goldmacher VS. Cell killing by antibody-drug conjugates. Cancer Lett. 2007; 255(2): 232–40. [PubMed: 17553616]
8. Loganzo F, Sung M, Gerber HP. Mechanisms of Resistance to Antibody-Drug Conjugates. Molecular cancer therapeutics. 2016; 15(12):2825–34. [PubMed: 27780876]
9. Winter G, Harris WJ. Humanized antibodies. Immunol Today. 1993; 14(6):243–246. [PubMed: 8397764]
10. Tjandra JJ, Ramadi L, McKenzie IF. Development of human anti-murine antibody (HAMA) response in patients. Immunol Cell Biol. 1990; 68(Pt 6):367–376. [PubMed: 1711007]
11. Nayak TK, Brechbiel MW. Radioimmunoimaging with longer-lived positron-emitting radionuclides: potentials and challenges. Bioconjug Chem. 2009; 20(5):825–841. [PubMed: 19125647]
12. Kaur S, Venktaraman G, Jain M, Senapati S, Garg PK, Batra SK. Recent trends in antibody-based oncologic imaging. Cancer Lett. 2012; 315(2):97–111. [PubMed: 22104729]

13. Holland JP, Williamson MJ, Lewis JS. Unconventional nuclides for radiopharmaceuticals. Mol Imaging. 2010; 9(1):1–20. [PubMed: 20128994]
14. Holland JP, Sheh Y, Lewis JS. Standardized methods for the production of high specific-activity zirconium-89. Nuclear medicine and biology. 2009; 36(7):729–39. [PubMed: 19720285]
15. Queern SL, Aweda TA, Massicano AVF, Clanton NA, El Sayed R, Sader JA, et al. Production of Zr-89 using sputtered yttrium coin targets (89)Zr using sputtered yttrium coin targets. Nuclear medicine and biology. 2017; 50:11–6. [PubMed: 28376350]
16. Zeglis BM, Houghton JL, Evans MJ, Viola-Villegas N, Lewis JS. Underscoring the influence of inorganic chemistry on nuclear imaging with radiometals. Inorganic chemistry. 2014; 53(4):1880–99. [PubMed: 24313747]
17. Deri MA, Zeglis BM, Francesconi LC, Lewis JS. PET imaging with (8)(9)Zr: from radiochemistry to the clinic. Nuclear medicine and biology. 2013; 40(1):3–14. [PubMed: 22998840]
18. Deri MA, Ponnala S, Zeglis BM, Pohl G, Dannenberg JJ, Lewis JS, et al. Alternative chelator for (8)(9)Zr radiopharmaceuticals: radiolabeling and evaluation of 3,4,3-(LI-1,2-HOPO). Journal of medicinal chemistry. 2014; 57(11):4849–60. [PubMed: 24814511]
19. Verel I, Visser GW, Boellaard R, Stigter-van Walsum M, Snow GB, van Dongen GA. 89Zr immuno-PET: comprehensive procedures for the production of 89Zr-labeled monoclonal antibodies. Journal of nuclear medicine : official publication, Society of Nuclear Medicine. 2003; 44(8):1271–81.
20. Perk LR, Vosjan MJ, Visser GW, Budde M, Jurek P, Kiefer GE, et al. p-Isothiocyanatobenzyl-desferrioxamine: a new bifunctional chelate for facile radiolabeling of monoclonal antibodies with zirconium-89 for immuno-PET imaging. European journal of nuclear medicine and molecular imaging. 2010; 37(2):250–9. [PubMed: 19763566]
21. Zeglis BM, Davis CB, Aggeler R, Kang HC, Chen A, Agnew BJ, et al. Enzyme-mediated methodology for the site-specific radiolabeling of antibodies based on catalyst-free click chemistry. Bioconjugate chemistry. 2013; 24(6):1057–67. [PubMed: 23688208]
22. Bhattacharyya S, Kurdziel K, Wei L, et al. Zirconium-89 Labeled Panitumumab: a Potential Immuno-PET Probe for HER1-Expressing Carcinomas. Nuclear medicine and biology.
23. Holland JP, et al. Measuring the pharmacodynamic effects of a novel Hsp90 inhibitor on HER2/neu expression in mice using Zr-89-DFO-trastuzumab. PLoS ONE. 2010; 5(1)
24. Bensch F, Lamberts LE, Smeenk MM, Jorritsma-Smit A, Lub-de Hooge MN, Terwisscha van Scheltinga AGT, de Jong JR, Gietema JA, Schröder CP, Thomas M, Jacob W, Abiraj K, Adessi C, Meneses-Lorente G, James I, Weisser M, Brouwers AH, de Vries EGE. PCSA 89Zr-Lumretuzumab PET Imaging before and during HER3 Antibody Lumretuzumab Treatment in Patients with Solid Tumors. Clin Canc Res. 2017; 23(20):6128–6137.
25. Holland JP, Divilov V, Bander NH, Smith-Jones PM, Larson SM, Lewis JS. 89Zr-DFO-J591 for immunoPET of prostate-specific membrane antigen expression in vivo. J Nucl Med. 2010; 51(8): 1293–300. [PubMed: 20660376]
26. Holland JP, Divilov V, Bander NH, Smith-Jones PM, Larson SM, Lewis JS. 89Zr-DFO-J591 for immunoPET of prostate-specific membrane antigen expression in vivo. J Nucl Med. 2010; 51(8): 1293–300. [PubMed: 20660376]
27. Perk LR, Visser OJ, Stigter-van Walsum M, et al. Preparation and evaluation of 89Zr-Zevalin for monitoring of 90Y-Zevalin biodistribution with positron emission tomography. European Journal of Nuclear Medicine and Molecular Imaging. 2006; 33(11):1337–1345. [PubMed: 16832633]
28. Vugts D, Heuveling D, Stigter-van Walsum M, et al. Preclinical evaluation of 89Zr-labeled anti-CD44 monoclonal antibody RG7356 in mice and cynomolgus monkeys: prelude to phase 1 clinical studies. MAbs. 2013; 6(2):567–575. [PubMed: 24492295]
29. England CG, Ehlerding EB, Hernandez R, Rekoske BT, Graves SA, Sun H, Liu G, McNeel DG, Barnhart TE, Cai W. Preclinical Pharmacokinetics and Biodistribution Studies of 89Zr-Labeled Pembrolizumab. J Nucl Med. 2017; 58(1):162–68. [PubMed: 27493273]
30. Cole EL, Kim J, Donnelly DJ, Smith RA, Cohen D, Lafont V, Morin PE, Huang RY, Chow PL, Hayes W, Bonacorsi S Jr. Radiosynthesis and preclinical PET evaluation of 89Zr-nivolumab (BMS-936558) in healthy non-human primates. Bioorg Med Chem. 2017; 25(20):5407–5414. [PubMed: 28803798]

31. Nagengast WB, de Vries EG, Hospers GA, et al. In vivo VEGF imaging with radiolabeled bevacizumab in a human ovarian tumor xenograft. JNM. 2007; 48(8):1313–1319. [PubMed: 17631557]
32. Larimer BM, Wehrenberg-Klee E, Dubois F, Mehta A, Kalomeris T, Flaherty K, Boland G, Mahmood U. Granzyme B PET Imaging as a Predictive Biomarker of Immunotherapy Response. Cancer Res. 2017; 77(9):2318–2327. [PubMed: 28461564]
33. McKnight B, Gibson H, Wei-Zen WeiVillegas NV. ImmunoPET imaging of functional marker interferon-gamma predicts adaptive response to tumor immunotherapy. Abstract presented at: World Molecular Imaging Society Annual Meeting; September 16, 2017; Philadelphia, PA.
34. Larimer BM, Wehrenberg-Klee E, Caraballo A, Mahmood Y. Quantitative CD3 PET Imaging Predicts Tumor Growth Response to Anti-CTLA-4 Therapy. JNM. 2016; 57(10):1607–1611. [PubMed: 27230929]
35. Tavaré R, McCracken MN, Zettlitz KA, Salazar FB, Olafsen T, Witte ON, Wu AM. Immuno-PET of Murine T Cell Reconstitution Postadoptive Stem Cell Transplantation Using Anti-CD4 and Anti-CD8 Cys-Diabodies. J Nucl Med. 2015; 56(8):1258–64. [PubMed: 25952734]
36. Houghton JL, Abdel-Atti D, Scholz WW, Jewis JS. Preloading with Unlabeled CA19.9 Targeted Human Monoclonal Antibody Leads to Improved PET Imaging with 89Zr-5B1. Mol Pharm. 2017; 6(14):908–915.
37. Lohrmann C, O'Reilly E, O'Donoghue J, Yu K, Pandit-Taskar N, Lyashchenko S, Ruan S, Wu J, DeNoble P, Carrasquillo J, Schmidtlein C, Teng R, Lowery M, Varghese A, Estrella H, Scholz W, Maffuid P, Lewis J, Weber W. First-in-Human Study of 89Zr-DFO-HuMab-5B1 (MVT-2163) PET/CT imaging with and without HuMab-5B1 (MVT-5873) in patients with pancreatic cancer and other CA 19–9 positive malignancies. J Nucl Med. 2017; 58(Supplement 1):385.
38. Borjesson PK, Jauw YW, Boellaard R, de Bree R, Comans EF, Roos JC, et al. Performance of immuno-positron emission tomography with zirconium-89-labeled chimeric monoclonal antibody U36 in the detection of lymph node metastases in head and neck cancer patients. Clinical cancer research : an official journal of the American Association for Cancer Research. 2006; 12(7 Pt 1): 2133–40. [PubMed: 16609026]
39. Siravegna G, Marsoni S, Siena S, Bardelli A. Integrating liquid biopsies into the management of cancer. Nat Rev Clin Oncol. 2017; 14(9):531–548. [PubMed: 28252003]
40. Lorenz JM. Updates in percutaneous lung biopsy: new indications, techniques and controversies. Semin Intervent Radiol. 2012; 29(4):319–324. [PubMed: 24293806]
41. El-Osta H, Hong D, Wheler J, et al. Outcomes of research biopsies in phase I clinical trials: the MD anderson cancer center experience. Oncologist. 2011; 16(9):1292–1298. [PubMed: 21859821]
42. Ben-Haim S, Ell P. 18F-FDG PET and PET/CT in the evaluation of cancer treatment response. J Nucl Med. 2009; 50(1):88–99. [PubMed: 19139187]
43. Pandit-Taskar N, O'Donoghue JA, Durack JC, et al. A Phase I/II Study for Analytic Validation of 89Zr-J591 ImmunoPET as a Molecular Imaging Agent for Metastatic Prostate Cancer. Clin Cancer Res. 2015; 21(23):5277–5285. [PubMed: 26175541]
44. Pandit-Taskar N, O'Donoghue JA, Ruan S, et al. First-in-Human Imaging with 89Zr-Df-IAB2M Anti-PSMA Minibody in Patients with Metastatic Prostate Cancer: Pharmacokinetics, Biodistribution, Dosimetry, and Lesion Uptake. J Nucl Med. 2016; 57(12):1858–1864. [PubMed: 27516450]
45. Dijkers EC, Oude Munnink TH, Kosterink JG, et al. Biodistribution of 89Zr-trastuzumab and PET imaging of HER2-positive lesions in patients with metastatic breast cancer. Clin Pharmacol Ther. 2010; 87(5):586–592. [PubMed: 20357763]
46. Oude Munnink TH, Dijkers EC, Netters SJ, et al. Trastuzumab pharmacokinetics influenced by extent human epidermal growth factor receptor 2-positive tumor load. J Clin Oncol. 2010; 28(21):e355–356. author reply e357. [PubMed: 20458048]
47. Bruno R, Washington CB, Lu JF, Lieberman G, Banken L, Klein P. Population pharmacokinetics of trastuzumab in patients with HER2+ metastatic breast cancer. Cancer Chemother Pharmacol. 2005; 56(4):361–369. [PubMed: 15868146]
48. Li C, Agarwal P, Gibiansky E, Jin JY, Dent S, Goncalves A, et al. A Phase I Pharmacokinetic Study of Trastuzumab Emtansine (T-DM1) in Patients with Human Epidermal Growth Factor

Receptor 2-Positive Metastatic Breast Cancer and Normal or Reduced Hepatic Function. Clin Pharmacokinet. 2017; 56(9):1069–80. [PubMed: 27995530]

49. Agus DB, Gordon MS, Taylor C, Natale RB, Karlan B, Mendelson DS, et al. Phase I clinical study of pertuzumab, a novel HER dimerization inhibitor, in patients with advanced cancer. Journal of clinical oncology : official journal of the American Society of Clinical Oncology. 2005; 23(11): 2534–43. [PubMed: 15699478]
50. Tran L, Baars JW, Aarden L, Beijnen JH, Huitema AD. Pharmacokinetics of rituximab in patients with CD20 positive B-cell malignancies. Hum Antibodies. 2010; 19(1):7–13. [PubMed: 20555126]
51. Jauw YW, Zijlstra JM, de Jong D, et al. Performance of 89Zr-Labeled-Rituximab-PET as an Imaging Biomarker to Assess CD20 Targeting: A Pilot Study in Patients with Relapsed/Refractory Diffuse Large B Cell Lymphoma. PLoS One. 2017; 12(1):e0169828. [PubMed: 28060891]
52. Ulaner GA, Hyman DM, Lyashchenko SK, Lewis JS, Carrasquillo JA. 89Zr-Trastuzumab PET/CT for Detection of Human Epidermal Growth Factor Receptor 2-Positive Metastases in Patients With Human Epidermal Growth Factor Receptor 2-Negative Primary Breast Cancer. Clin Nucl Med. 2017
53. Pan M, Gao D, Feng J, He J, Seo Y, Tedesco J, Wolodzko J, Hasegawa B, Franc B. Biodistributions of 177Lu- and 111In- labeled 7E11 Antibodies to Prostate-Specific Membrane Antigen in Xenograft Model of Prostate Cancer and Potential Use of 111In-7E11 as a Pretherapeutic agent for 177Lu-7E11 Radioimmunotherapy. Mol Imaging Biol. 2009; 11(3):159–166. [PubMed: 19034582]
54. Pai-Scherf L, Carrasquillo J, Paik C, Gansow O, Whatley M, Pearson D, Webber K, Hamilton M, Allegra C, Brechbiel M, Willingham M, Pastan I. Imaging and Phase I Study of 111In- and 90Y-labeled Anti-Lewis^{Y} Monoclonal Antibody B3. Clin Canc Res. 2000; 6(5):1720–1730.
55. Goins B, Bao A, Phillips W. Liposomes. Methods in Molecular Biology. Vol. 1522. Humana Press; New York, NY: Techniques for Loading Technetium-99m and Thenium-186/188 Radionuclides into Preformed Liposomes for Diagnostic Imaging and Radionuclide Therapy.
56. Heinzmann K, Carter LM, Lewis JS, Aboagye EO. Multiplexed imaging for diagnosis and therapy. Nature Biomedical Engineering. 2017; 1(9):697–713.
57. Severin GW, Engle JW, Barnhart TE, Nickles RJ. 89Zr radiochemistry for positron emission tomography. Med Chem. 2011; 7(5):389–394. [PubMed: 21711221]
58. Rizvi SN, Visser OJ, Vosjan MJ, et al. Biodistribution, radiation dosimetry and scouting of 90Y-ibritumomab tiuxetan therapy in patients with relapsed B-cell non-Hodgkin's lymphoma using 89Zr-ibritumomab tiuxetan and PET. Eur J Nucl Med Mol Imaging. 2012; 39(3):512–520. [PubMed: 22218876]
59. Rahmim A, Zaidi H. PET versus SPECT: strengths, limitations and challenges. Nuclear medicine communications. 2008; 29(3):193–207. [PubMed: 18349789]
60. Chun SY, Fessler JA, Dewaraja YK. Correction for collimator-detector response in SPECT using point spread function template. IEEE transactions on medical imaging. 2013; 32(2):295–305. [PubMed: 23086521]
61. Carrasquillo JA, White JD, Paik CH, et al. Similarities and differences in 111In- and 90Y-labeled 1B4M-DTPA antiTac monoclonal antibody distribution. J Nucl Med. 1999; 40(2):268–276. [PubMed: 10025834]
62. Lamberts LE, Menke-van der Houven van Oordt CW, ter Weele EJ, et al. ImmunoPET with Anti-Mesothelin Antibody in Patients with Pancreatic and Ovarian Cancer before Anti-Mesothelin Antibody-Drug Conjugate Treatment. Clin Cancer Res. 2016; 22(7):1642–1652. [PubMed: 26589435]
63. Gebhart G, Lamberts LE, Wimana Z, et al. Molecular imaging as a tool to investigate heterogeneity of advanced HER2-positive breast cancer and to predict patient outcome under trastuzumab emtansine (T-DM1): the ZEPHIR trial. Ann Oncol. 2016; 27(4):619–624. [PubMed: 26598545]
64. Gaykema SB, Schroder CP, Vitfell-Rasmussen J, et al. 89Zr-trastuzumab and 89Zr-bevacizumab PET to evaluate the effect of the HSP90 inhibitor NVP-AUY922 in metastatic breast cancer patients. Clinical cancer research : an official journal of the American Association for Cancer Research. 2014; 20(15):3945–3954. [PubMed: 25085789]

65. Menke-van der Houven van Oordt CW, Gootjes EC, Huisman MC, et al. 89Zr-cetuximab PET imaging in patients with advanced colorectal cancer. Oncotarget. 2015; 6(30):30384–30393. [PubMed: 26309164]
66. Laforest R, Lapi SE, Oyama R, et al. [89Zr]Trastuzumab: Evaluation of Radiation Dosimetry, Safety, and Optimal Imaging Parameters in Women with HER2-Positive Breast Cancer. Mol Imaging Biol. 2016; 18(6):952–959. [PubMed: 27146421]
67. Lindenberg L, Adler S, Turkbey IB, et al. Dosimetry and first human experience with 89Zr-panitumumab. Am J Nucl Med Mol Imaging. 2017; 7(4):195–203. [PubMed: 28913158]
68. Quinn B, Dauer Z, Pandit-Taskar N, Schoder H, Dauer LT. Radiation dosimetry of 18F-FDG PET/CT: incorporating exam-specific parameters in dose estimates. BMC Med Imaging. 2016; 16(1):41. [PubMed: 27317478]
69. Tolmachev V, Velikyan I, Sandstrom M, Orlova A. A HER2-binding Affibody molecule labelled with 68Ga for PET imaging: direct in vivo comparison with the 111In-labelled analogue. Eur J Nucl Med Mol Imaging. 2010; 37(7):1356–1367. [PubMed: 20130858]
70. Xavier C, Blykers A, Vaneycken I, et al. (18)F-nanobody for PET imaging of HER2 overexpressing tumors. Nucl Med Biol. 2016; 43(4):247–252. [PubMed: 27067045]
71. Su X, Cheng K, Liu Y, Hu X, Meng S, Cheng Z. PET imaging of insulin-like growth factor type 1 receptor expression with a 64Cu-labeled Affibody molecule. Amino Acids. 2015; 47(7):1409–1419. [PubMed: 25854877]
72. Garousi J, Andersson KG, Mitran B, et al. PET imaging of epidermal growth factor receptor expression in tumours using 89Zr-labelled ZEGFR:2377 affibody molecules. Int J Oncol. 2016; 48(4):1325–1332. [PubMed: 26847636]
73. Eder M, Knackmuss S, Le Gall F, et al. 68Ga-labelled recombinant antibody variants for immuno-PET imaging of solid tumours. Eur J Nucl Med Mol Imaging. 2010; 37(7):1397–1407. [PubMed: 20157706]
74. Lutje S, Franssen GM, Sharkey RM, et al. Anti-CEA antibody fragments labeled with [(18)F]AlF for PET imaging of CEA-expressing tumors. Bioconjug Chem. 2014; 25(2):335–341. [PubMed: 24382090]
75. Wong P, Li L, Chea J, et al. Synthesis, Positron Emission Tomography Imaging, and Therapy of Diabody Targeted Drug Lipid Nanoparticles in a Prostate Cancer Murine Model. Cancer Biother Radiopharm. 2017; 32(7):247–257. [PubMed: 28910151]
76. Zettlitz KA, Tavare R, Knowles SM, Steward KK, Timmerman JM, Wu AM. ImmunoPET of malignant and normal B cells with 89Zr- and 124I-labeled obinutuzumab antibody fragments reveals differential CD20 internalization in vivo. Clin Cancer Res. 2017
77. Viola-Villegas NT, Sevak KK, Carlin SD, et al. Noninvasive Imaging of PSMA in prostate tumors with (89)Zr-Labeled huJ591 engineered antibody fragments: the faster alternatives. Mol Pharm. 2014; 11(11):3965–3973. [PubMed: 24779727]
78. Knowles SM, Tavare R, Zettlitz KA, et al. Applications of immunoPET: using 124I-anti-PSCA A11 minibody for imaging disease progression and response to therapy in mouse xenograft models of prostate cancer. Clin Cancer Res. 2014; 20(24):6367–6378. [PubMed: 25326233]
79. AJ, Cao PJ, Hedley DW, Sidhu SS, Winnik MA, Reilly RM. MicroPET/CT imaging of patient-derived pancreatic cancer xenografts implanted subcutaneously or orthotopically in NOD-scid mice using (64)Cu-NOTA-panitumumab F(ab')2 fragments. Nucl Med Biol. 2015; 42(2):71–77. [PubMed: 25456837]

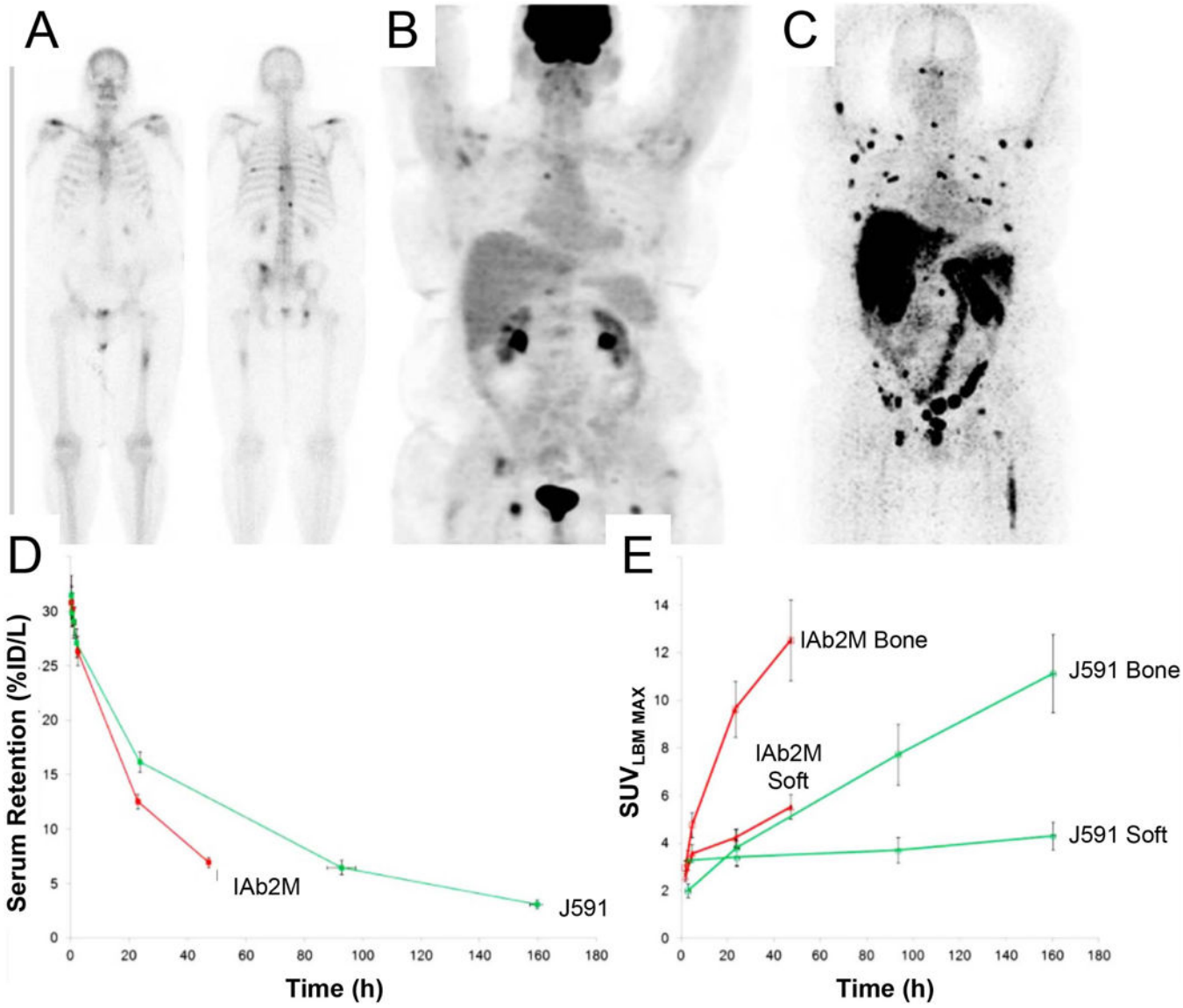

Figure 1. Confirmation of Malignancy

Differences in lesion detection in a metastatic prostate cancer patient using ^{99m}Tc-MDP (bone scan) showed lesions in the ribs and vertebrae A), ^{18}F-FDG PET scan displayed uptake in the femur and in the vertebrae B), and ^{89}Zr-IAB2M imaging identified more true-positive lesions than ^{99m}Tc-MDP and ^{18}F-FDG C). **Optimization of pharmacokinetics.** A comparison of serum clearance D) and lesion uptake E) between ^{89}Zr-IAB2M (minibody) and ^{89}Zr-J591 (full length mAb cognate) over time. This research was originally published at JNM Pandit-Taskar N,Donoghue JA, Ruan S, et al. First-in-Human Imaging with ^{89}Zr-Df-IAB2M Anti-PSMA Minibody in Patients with Metastatic Prostate Cancer: Pharmacokinetics, Biodistribution, Dosimetry, and Lesion Uptake. J Nucl Med.2016;57(12): 1858–1864. © by the Society of Nuclear Medicine and Molecular Imaging, Inc. (reprinted with permission from ref.44).

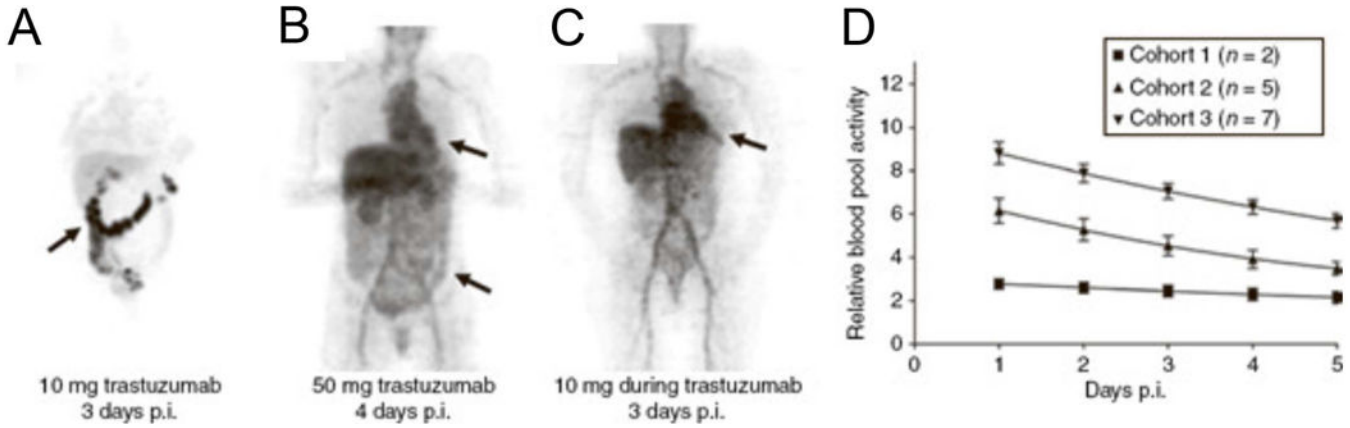

Figure 2. Receptor occupancy

^{89}Zr-trastuzumab PET biodistribution in patients given 10 mg of ^{89}Zr-trastuzumab (untreated) A), 50 mg ^{89}Zr-trastuzumab during concurrent trastuzumab treatment B), and 10 mg ^{89}Zr-trastuzumab during concurrent trastuzumab treatment C) show different clearance rates in the blood pool D), and should be considered when dosing patients in the clinic. This research was originally published at Clin Pharmacol Ther. Dijkers EC, Oude Munnink TH, Kosterink JG, et al. Biodistribution of ^{89}Zr-trastuzumab and PET imaging of HER2-positive lesions in patients with metastatic breast cancer. Clin Pharmacol Ther. 2010;87(5):586–592. (reproduced with permission from Wiley © ref.45)

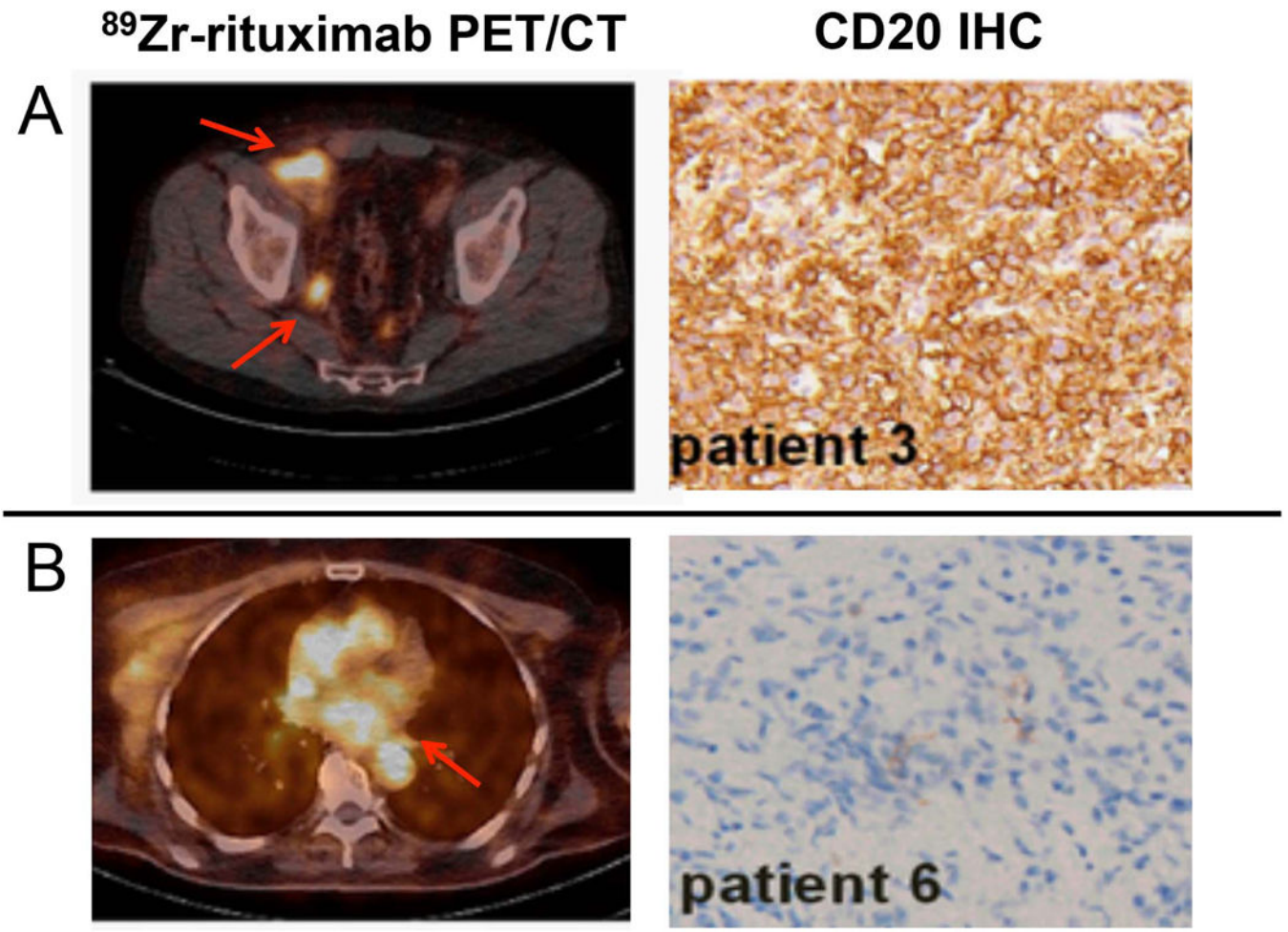

Figure 3. ImmunoPET findings in relation to pathology

Concordance A) and B) discordance of ^{89}Zr-rituximab-PET/CT (left) with CD20 pathology via IHC (right). Arrows point to lesions on the PET scan. This research was originally published at PLOS One Jauw YW, Zijlstra JM, de Jong D, et al. Performance of ^{89}Zr-Labeled-Rituximab-PET as an Imaging Biomarker to Assess CD20 Targeting: A Pilot Study in Patients with Relapsed/Refractory Diffuse Large B Cell Lymphoma. PLoS One. 2017;12(1):e0169828 and modified for use under the creative commons license https://creativecommons.org/licenses/by/4.0/).

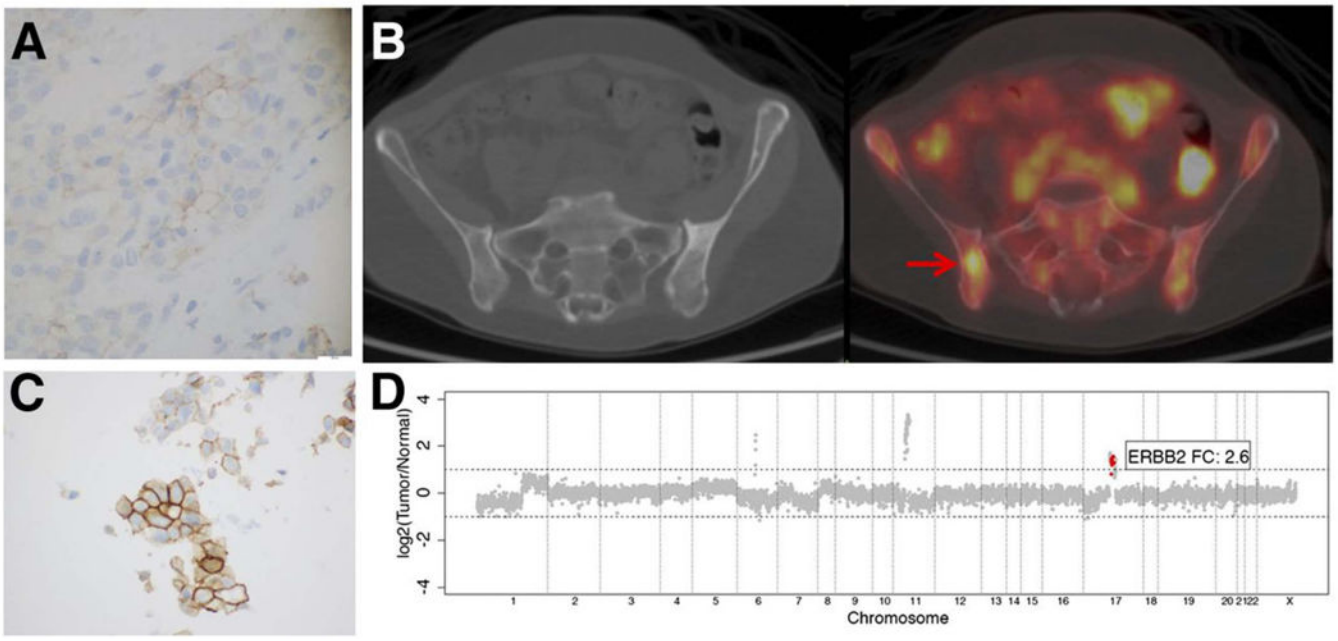

Figure 4.

PET readout gave true-positive results despite discordance with biopsy findings. An ER+/HER2- invasive ductal BC patient with confirmed negative pathology in the primary lesion A) but presented with HER2-PET positive disease 2 years after primary diagnosis B). Biopsy of the same site resulted an ambiguous IHC score (2+) C). MSK-IMPACT assay confirmed the foci as truepositive D). Arrows point to lesions. This research was originally published in JNM. Ulaner GA, Hyman DM, Ross DS, et al. Detection of HER2-Positive Metastases in Patients with HER2-Negative Primary Breast Cancer Using 89Zr-Trastuzumab PET/CT. Journal of nuclear medicine : official publication, Society of Nuclear Medicine. 2016;57(10):1523–1528. ©1by the Society of Nuclear Medicine and Molecular Imaging, Inc.(reproduced with permission from Ref. 52)

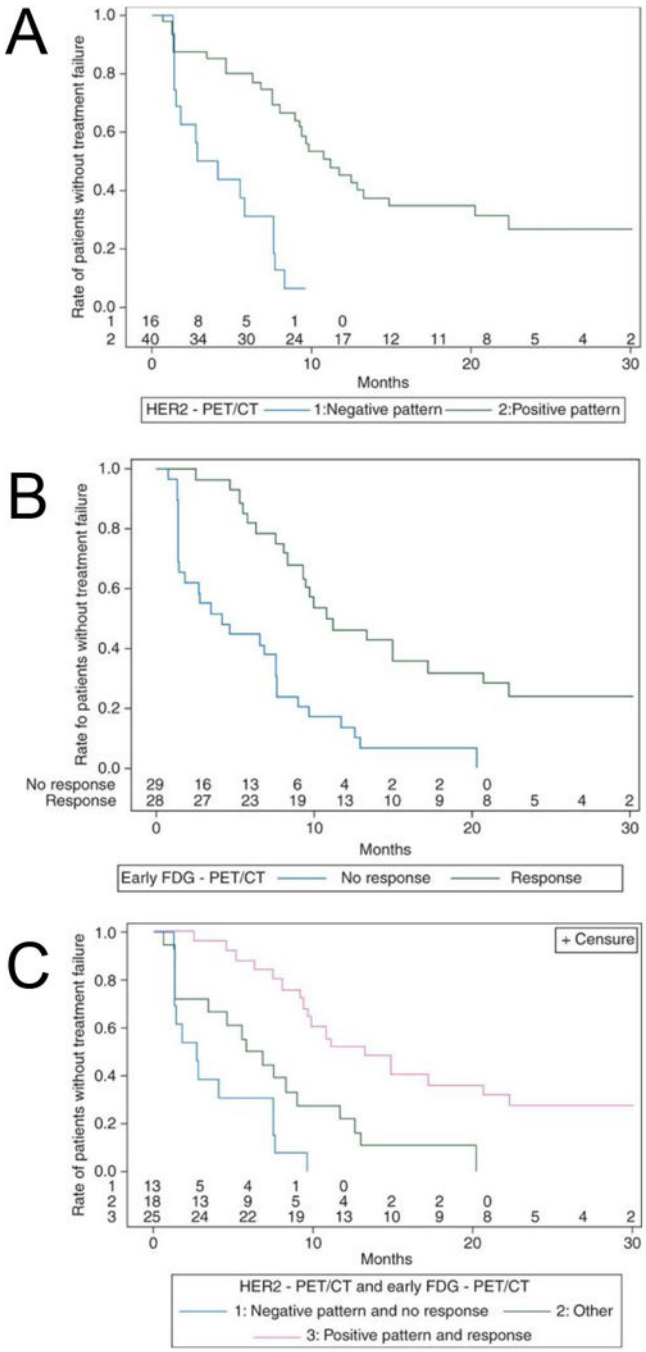

Figure 5. Predictive Markers of Treatment

Time-to-treatment failures were evaluated based on HER2-PET/CT A), early FDG-PET/CT B) and combination of both HER2- and FDG-PET/CT C). This research was originally published in Ann Oncol. Gebhart G, Lamberts LE, Wimana Z, et al. Molecular imaging as a tool to investigate heterogeneity of advanced HER2-positive breast cancer and to predict patient outcome under trastuzumab emtansine (T-DM1): the ZEPHIR trial. Ann Oncol. 2016;27(4):619–624. (Reproduced with permission From Oxford University Press Ref. 63).

Table 1

Different antibody fragments and recommended PET radionuclide for companion diagnostic development.

Antibody Fragments	Recommended PET Nuclide	References
Affibody (~7 kDa), Nanobody (~12–15 kDa)	^{68}Ga ^{18}F ^{64}Cu	69–73
Diabody (~55 kDa)	^{18}F ^{64}Cu ^{89}Zr	74–76
Minibody (~80 kDa)	^{64}Cu ^{89}Zr	77–78
Fab'$_2$ (~100–110 kDa)	^{64}Cu ^{89}Zr ^{124}I	79

Table 2

List of ^{89}Zr-immunoPET tracers that advanced to clinical trials

ANTIBODY	TARGET	INDICATIONS	CLINICALTRIALS.GOV IDENTIFIER	PHASE AND STATUS
Trastuzumab	HER2	Metastatic HER2+ Breast cancer	NCT01420146	Phase 1, Completed
		Metastatic HER2+ Breast cancer; to select patients for T-DM1 treatment	NCT01565200	Phase 2, Active, not recruiting
		Unsuspected HER2 Breast Metastases	NCT02286843	Recruiting
		Trastuzumab-resistant Breast Cancer; measure HER2 post-treatment with HSP90 inhibitor AUY922	NCT01081600	Phase 1/2, Completed
		Esophagogastric cancer	NCI-2016–00986, NCT02023996	Phase 1; Recruiting
		HER2+ primary malignancy	NCT03109977	On-going but not recruiting
Ibritumomab Tiuxetan	CD20	Non-hodgkins lymphoma		Complete
Bevacizumab	VEGF	Inflammatory Breast Cancer	NCT01894451	Phase 1; recruiting
		Pulmonary arterial hypertension	NCT03166306	Phase 1/2; not open to recruitment at the time of writing
huJ591	PSMA	Prostate cancer	NCT02693860	Phase 1; recruiting
		Metastatic prostate cancer	NCT01543659	Phase 1/2; On-going but not recruiting
		Glioblastoma	NCT02410577	Phase I, On-going but not recruiting
Girentuximab	Carbonic Anydrase IX	Renal cell carcinoma	NCT02883153	Phase 2/3, Completed
Cetuximab	EGFR	Stage IV cancer	NCT00691548	Phase 1; Completed
		Colorectal cancer	NCT01691391	Completed
Ipilimumab	CTLA-4	Melanoma	NCT03313323	Phase 2; Recruiting
Fresolimumab (GC1008)	TGF-β	Primary brain tumor	NCT01472731	Phase 2; Completed
U36	CD44v6	Head and neck cancer		Completed
Pertuzumab	HER2	HER2 positive malignancy	NCT03109977	Phase 1; On-going but not recruiting
IAb2M	PSMA	Metastatic prostate cancer	NCT01923727	Phase 1/2, Completed
		Prostate cancer, pre-prostatectomy	NCT02349022	Phase 2, Completed
IAb22M2C	CD8	Non Small Cell Lung Cancer, Small Cell Lung Cancer, Squamous Cell Carcinoma Head and Neck, Melanoma, Merkel Cell Tumor, Renal, Bladder, Hepatocellular, Triple Negative Breast, or Gastroesophageal Cancer, Hodgkin's Lymphoma	NCT03107663	Phase 1, Recruiting
Rituximab	CD20	Lung disease, interstitial pneumonitis	NCT02251964	Phase 2/3; On-going but not recruiting
GSK3128349 (Albumin domain binding antibody)	Albumin	Drug related side effects and adverse reactions	NCT02829307	Phase 1; completed
MPDL3280	PD-L1	Breast cancer, bladder cancer and non small cell lung cancer	NCT02453984	Phase 1; recruiting

ANTIBODY	TARGET	INDICATIONS	CLINICALTRIALS.GOV IDENTIFIER	PHASE AND STATUS
Pembrolizumab	PD-1	Non small cell lung cancer	NCT03065764	Phase 2; on-going but not recruiting
GSK2849330	HER3	Solid tumors	NCT02345174	Phase 1; Completed
AMG211	HER3	Advanced gastrointestinal cancer	NCT02760199	Phase 1; Completed
RO5479599	HER3	Metastatic and/or Locally Advanced Malignant HER3-Positive Solid Tumors of Epithelial Cell Origin	NCT01482377	Phase 1; Completed
MMOT0530A	Mesothelin	Unresectable pancreatic cancer, platinum-resistant ovarian cancer	NCT01832116	Phase 1; Completed
MSTP2109A	STEAP1	Prostate cancer	NCT01774071	Phase 1/2; On-going but not recruiting
HuMab-5B1 (MVT-2163)	CA19.9	Pancreatic Cancer; tumors that express CA19.9	NCT02687230	Phase 1; Recruiting